



High frequency torsional-mode nanomechanical resonators enabled by very thin nanocrystalline diamond diaphragms



Rui Yang, Christian A. Zorman, Philip X.-L. Feng*

Department of Electrical Engineering & Computer Science, Case School of Engineering, Case Western Reserve University, 10900 Euclid Avenue, Cleveland, OH 44106, USA

ARTICLE INFO

Available online 5 December 2014

Keywords:

Nanocrystalline diamond
Micro/nanoelectromechanical systems (MEMS/NEMS)
Torsional resonator
Focused ion beam (FIB)
High frequency
Young's modulus

ABSTRACT

We report an experimental demonstration of high-frequency (HF) torsional-mode nanomechanical resonators based on nanocrystalline diamond films as thin as 50 nm. Devices axially supported by pairs of tethers as small as 90 nm × 50 nm in cross section are fabricated from suspended diaphragms by using focused ion beam (FIB), showing multi-mode resonances with frequencies (f_{res}) into the HF band (up to ~10 MHz, while most existing sensitive torsional devices are at kHz or low-MHz), and quality (Q) factors exceeding 1800 at room temperature in moderate vacuum (~20 mTorr). This fabrication process evades the conventional electron-beam lithography and etching steps that are destructive for very thin diaphragms. From the torsional and flexural modes of device resonances, we calculate Young's modulus (E_V) to be as high as 977 GPa, which is almost comparable to the known value of 1220 GPa for single-crystal diamond.

© 2014 Elsevier B.V. All rights reserved.

1. Introduction

Diamond has been a particularly attractive and interesting material for constructing micro/nanoelectromechanical systems (MEMS/NEMS) because of its exceptional mechanical properties (Young's modulus up to 1220 GPa), and relatively low mass density (3500 kg/m³), which provides a high acoustic velocity resulting in high frequency mechanical resonators [1–3]. Its very high thermal conductivity (22 W/(cm·K)), and excellent wear/corrosion resistivity make diamond suitable for sensing, signal processing and communication in harsh environments [4]. As device dimensions scale down for applications that require higher sensitivity or higher speed, thin films of diamond have been grown by techniques such as microwave plasma chemical vapor deposition (MPCVD) [5,6], or hot filament chemical vapor deposition (HFCVD) [7,8], showing material properties comparable to single crystal diamond. Resonant structures based on polycrystalline, nanocrystalline, and ultrananocrystalline diamond films have been explored [8–17], demonstrating both high frequency (HF) and high quality (Q) factor resonators.

Torsional resonators are usually composed of a pair of tethers that support a paddle, with the paddle rotating with respect to the center line defined by the tethers. These devices are particularly interesting for sensing applications because high frequency can be achieved by the miniaturized tethers, while adequate capturing area can be realized by the rotating paddles [18,19]. Various sensing applications have been demonstrated based on torsional resonators [20–31], demonstrating the capability of this type of device design. These devices are mainly built on Si and SiN layers and fabricated by electron-beam lithography

or photolithography, or with carbon nanotubes grown by bottom-up synthesis, which require careful chemical processing or etching. It would be desirable to explore torsional devices beyond these materials that are compatible with sensing in harsh environments. Towards this goal, we have explored torsional resonators using a 'smart-cut' 1.2 μm-thick 6H-SiC film [32] that is suitable for harsh environment applications, and demonstrated photon sensing with these devices [33]. Now we extend the technology to diamond thin films grown by CVD that are as thin as 50 nm while maintaining desirable material properties. Torsional resonators based on polycrystalline diamond have been demonstrated [11]; however, torsional devices based on diamond thin films showing resonances in the HF band have not yet been developed.

In this work, we demonstrate the first double-tether-supported nanocrystalline diamond torsional resonators with high resonance frequencies. We fabricate torsional resonators on 50 to 100 nm thin nanocrystalline diamond films with tether dimensions as small as 50 nm × 90 nm in cross section, and torsional paddles typically 5 μm × 2 μm in area. Focused ion beam (FIB) is carefully adjusted to fabricate the devices on suspended diaphragms, avoiding several challenging chemical processing steps that can adversely affect fabrication yield. Raman spectroscopy is performed on both suspended and non-suspended areas for films with different thicknesses to assess the quality of the diamond films. We measure multimode resonances of both undriven thermomechanical motions and the optically driven vibrations of these devices with laser interferometry, which show torsional resonances up to 8.4 MHz and Q's over 1800. From the resonance frequency of the torsional mode, we estimate Young's modulus $E_V \approx 977$ GPa which is close to single crystal diamond. We also calibrate the device performance at different pressures from 25 mTorr to atmosphere pressure, and observe the effect of air damping at pressure higher than 1 Torr.

* Corresponding author.
E-mail address: philip.feng@case.edu (P.X.-L. Feng).

2. Device design and basic theory

The device has a torsional paddle supported by a pair of thin parallel tethers. For torsional motion, the tethers and the torsional paddles rotate around the axis defined by the two tethers, as shown in Fig. 1(a). Figure 1(b) illustrates the simulation result of the torsional mode shape by finite element modeling (FEM), which is consistent with Fig. 1(a): as one side of the paddle rotates up, the other side moves down, and the center of the paddle in line with the tethers does not move. The governing differential equation for torsional resonance is expressed as

$$\rho \frac{\partial^2 \theta}{\partial t^2} = G \frac{\partial^2 \theta}{\partial x^2}, \quad (1)$$

where ρ is the mass density, $G = E_Y/2(\gamma_P + 1)$, and γ_P is Poisson's ratio [34]. The equation can be rewritten as

$$\frac{\partial^2 \theta}{\partial t^2} = a^2 \frac{\partial^2 \theta}{\partial x^2}, \quad (2)$$

where $a = \sqrt{G/\rho}$, which is similar to the case of the flexural mode. The resonance frequency of a torsional resonator can be expressed as

$$f_{res} = \frac{1}{2\pi} \sqrt{\frac{2J_T G}{L_T I}}, \quad (3)$$

where L_T is the tether length and J_T is the torsional area moment of inertia, which for rectangular cross section is

$$J_T = w_T t^3 \times \left(\frac{1}{3} - 0.21 \times \frac{t}{w_T} \times \left(1 - \frac{w_T^4}{12 \times t^4} \right) \right), \quad (4)$$

where w_T is the tether width, t is the film thickness. I is the total mass moment of inertia from both the tethers and the paddle which is given by:

$$I = I_{tether} + I_{paddle} = \frac{1}{6} \rho t L_T w_T (w_T^2 + t^2) + \frac{1}{12} \rho t w L^3, \quad (5)$$

where w is the paddle width and L is the paddle length [35,36].

According to the above Eq. (4), for the thickness range we consider (1–50 nm), J_T increases with increasing t , while from Eq. (5) I also increases with t . Since the resonance frequency increases with higher J_T , but decreases with higher I , there is a tradeoff. As shown in Fig. 1(c), the torsional-mode resonance frequency (f_{res}) of this particular device we choose does not change monotonically with film thickness; instead, only at thickness greater than ~15 nm, f_{res} increases with increasing t , while for films thinner than ~15 nm, f_{res} increases with lowering thickness. Meantime, f_{res} is also related to multiple device parameters, such

as Young's modulus (E_Y) of the material, the tether width w_T , tether length L_T , and paddle size L and w . Diamond has very high Young's modulus and low mass density, thus it has interesting potential for high frequency and high quality (Q) factor devices. Further, thinner devices are desirable for achieving better sensitivity when we use the device as force, torque or inertia sensors [32]. Therefore here we use very thin nanocrystalline diamond films for fabricating the devices.

3. Experiments

3.1. Device fabrication processes

Fabrication of the torsional resonators starts from nanocrystalline diamond films provided by Applied Diamond Inc.TM that were deposited by a MPCVD technique on Si substrates [37]. The suspended diaphragms are obtained by attaching a plastic etch mask on the back side of Si and performing isotropic wet etching with a HF/HNO₃ mixture (Fig. 2). Then FIB is performed with 30 kV and 10 pA Ga⁺ ions to pattern the devices. Compared to electron-beam lithography that requires patterning on the substrate-supported film and then releasing the device with etching, this technique has a higher likelihood of obtaining suspended structures once FIB parameters are properly determined. Even if the fragile diaphragms are broken due to handling or previous etching steps, suspended devices can still be fabricated on patches of the broken diamond diaphragms with careful FIB processing. This high-resolution FIB method avoids many of the chemical processes associated with electron-beam lithography, enabling rapid prototyping of device structures with small dimensions. Torsional devices are fabricated on both 50 nm thick and 100 nm thick broken nanocrystalline diamond diaphragms.

The FIB process requires careful engineering to successfully fabricate suspended torsional devices with thin tethers (Fig. 3). Low ion beam current is necessary so that in the milling process the ion beam pressure on the film does not easily tilt or twist the device since the broken films are quite pliable. Furthermore, optimizing the sequence of patterning is required so that the pressure on the film or stress in the film is more evenly distributed to prevent the FIB area from moving relative to the desired location of the device being fabricated. Fig. 3(a) shows our initial attempt in milling all the parts enclosed in the orange border in a single FIB sequence using a beam current of ~50 pA. The resulting device is pictured in Fig. 3(b), showing that the initial fabrication approach is not successful because the entire device is twisted and the tethers are malformed. We improve the process by performing FIB sequentially with the individual steps indicated by the numbers 1–10 in Fig. 3(c). Process steps 5–8 are repeated several times to gradually narrow the tethers, which induces minimal stress on the film because only a small amount of the film is milled away during each step. This method efficiently yields torsional diamond resonators with very thin tethers (Fig. 3(d)). We could also add more FIB steps to mill away the surrounding area

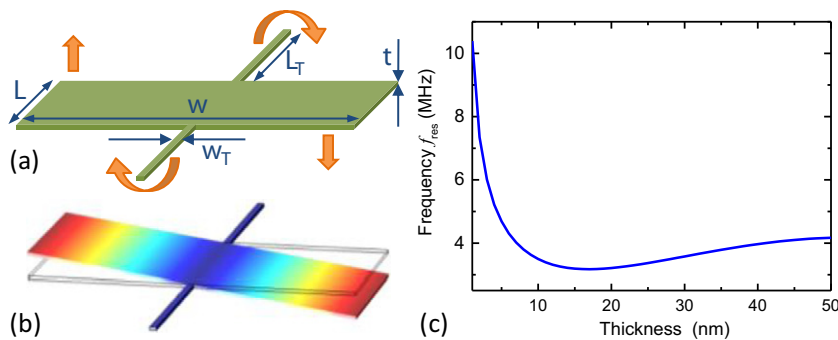


Fig. 1. Conceptual renderings of the diamond torsional resonators. (a) Illustration of the designed torsional resonator, with arrows showing the tether and paddle rotation. (b) FEM simulation of the torsional mode shape using COMSOL. (c) Dependence of the torsional mode resonance frequency on the film thickness. The parameters used are: $E_Y = 977$ GPa, Poisson ratio $\nu_P = 0.069$, $L_T = 2 \mu\text{m}$, $w_T = 50$ nm, $L = 2 \mu\text{m}$, $w = 5 \mu\text{m}$.

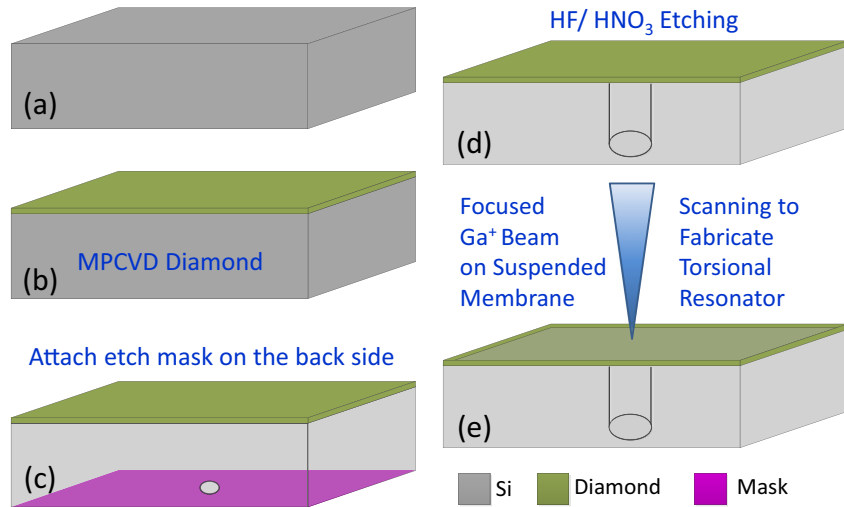


Fig. 2. Fabrication process of the diamond torsional resonators. (a) Si substrate. (b) MPCVD diamond. (c) Attaching a plastic film with a hole in the middle to the back side of the wafer as etch mask. (d) Isotropic etching of the Si through the mask using HF/HNO₃ mixture to form suspended diamond diaphragm. (e) FIB milling on the suspended diaphragm to fabricate torsional resonators.

near the device to minimize the interference during measurement. Even though there are several carefully engineered small steps in the course of the FIB, the entire process is not time-consuming, because the film is very thin and each actual milling step only takes 1–2 min, and also because today's state-of-the-art FIB (e.g., FEI NanoBuilder™) allows us to do CAD designs of arrays of complex structures for fast and high-throughput FIB processing with very high resolution. In this particular case, for patterning very small devices with nanoscale features, as shown in Fig. 3(d), from very thin suspended diaphragms, FIB processing exhibits salient advantages over electron-beam lithography, which will be very destructive when implemented on such suspended thin diaphragms. Given the starting diaphragm structures, high-resolution FIB processing is probably the best option to achieve the design goals and avoid all the undesirable wet chemical processes associated with conventional lithography. It would be formidably challenging to yield

similar devices by employing electron-beam lithography and etching processes on these very thin diaphragms.

3.2. Raman spectroscopy of the film

We assess the quality of the CVD diamond films by Raman spectroscopy with a 532 nm laser. Raman spectra are recorded on both suspended and Si-supported areas for the 50 nm (Fig. 4(a) and (b)) and 100 nm (Fig. 4(c) and (d)) thick films for comparison. Results show that the suspended film in Fig. 4(b) has the highest quality, since the peak around 1330 cm⁻¹ confirming the diamond phase [38] is most prominent (Fig. 4(b)).

From the spectrum in Fig. 4(b), we also observe trans-polyacetylene (1134 cm⁻¹ and 1463 cm⁻¹) peaks and amorphous carbon peaks (D peak: 1359 cm⁻¹, G peak: 1538 cm⁻¹) which are common in

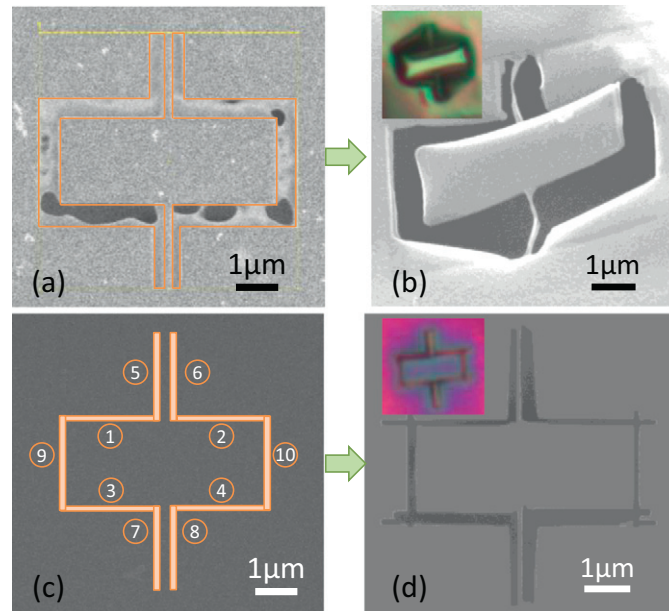


Fig. 3. FIB process for unsuccessful (a–b) and successful (c–d) devices. (a) Ion beam imaging where the area in the orange box indicates the area that is milled at the same time. (b) Tilted SEM image of the device, showing that it is twisted after fabrication and additional milling could totally remove the tethers. (c) SEM image of the film before fabrication with numbers 1–10 indicating the sequence to mill the respective area for a successful FIB process. (d) Top-view SEM image of the yielded device, with tethers as narrow as 90 nm. Insets in (b) & (d) show the optical microscope images of the devices.

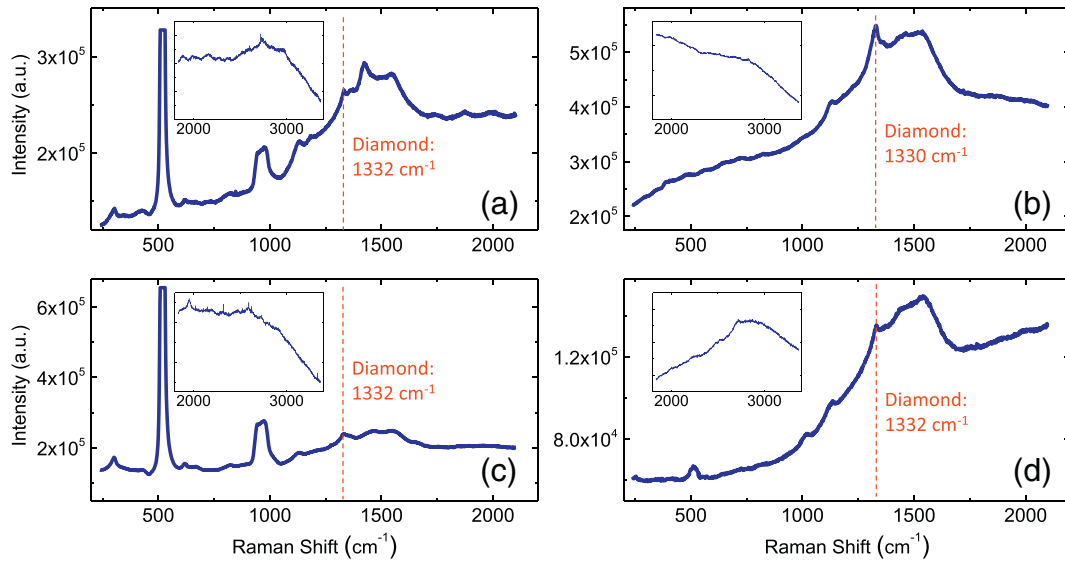


Fig. 4. Raman spectra of 50 nm thin (a & b) and 100 nm thin (c & d) nanocrystalline diamond films, where (a) & (c) are taken from the film on Si substrate, and (b) & (d) are taken from the suspended films. Insets show the Raman spectra at higher wave numbers.

nanocrystalline diamond films [39,40]. The Raman spectrum for the film on Si (Fig. 4(a)) also shows Si Raman peaks around 520 cm^{-1} and 960 cm^{-1} (indicating second-order scattering) in addition to the peaks observed in the suspended area shown in Fig. 4(b). For the spectra shown in Fig. 4(c) (unsuspended) and Fig. 4(d) (suspended), diamond peaks around 1332 cm^{-1} are also observed, but are not as notable as the films shown in Fig. 4(b), indicating that the crystal quality is not as high. The Raman spectra for higher wavenumbers are also shown as a reference, but we do not observe obvious second-order Raman spectra of diamond.

3.3. Mechanical resonance measurement

We measure the resonance characteristics of the nanocrystalline diamond torsional resonators with optical interferometry by using a 633 nm He–Ne red laser with an on-device spot size of $\sim 1\text{ }\mu\text{m}$. The undriven thermomechanical motion signal is collected with a photodetector and recorded with a spectrum analyzer (Agilent E4440A), using the measurement setup detailed in our previous work [33,41] (not shown here). The devices are placed in a vacuum chamber with an optical window to allow the laser to pass through, and the measurement is performed at room temperature and in vacuum ($\sim 20\text{ mTorr}$).

We also drive the device motion with a modulated 405 nm blue laser by focusing the laser close to the device. The laser is controlled by a

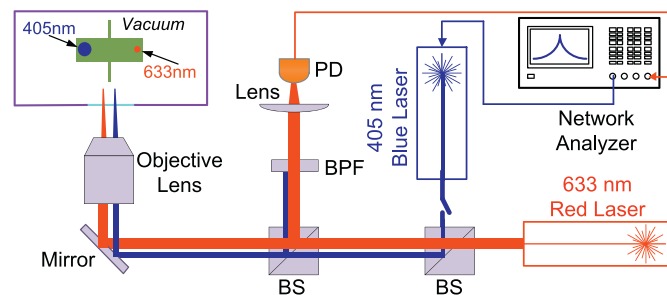


Fig. 5. Resonance measurement setup for optical driving with modulated 405 nm blue laser and detection with optical interferometry (633 nm red laser), where BS denotes beam splitter, and BPF stands for band pass filter allowing red laser to pass through while blocking the blue laser. To measure undriven thermomechanical motion, the blue laser could be turned off and the signal from the photodetector should be connected to the spectrum analyzer.

radio-frequency (RF) network analyzer (HP 3577A) to sweep the driving frequency, and an amplitude-modulated laser with a photon energy of 3.07 eV effectively induces periodic heating in the device, driving the device through thermal expansion and consequent periodic motion (Fig. 5). To drive the torsional mode motion of the device, we usually focus the blue laser at one end of the paddle, and the red detection laser on the other end of the paddle to minimize the effect of the blue laser background on the detection signal. When the driving frequency is close to the resonance frequency of the device, the device motion will be large. The signal is detected by the 633 nm laser, and recorded

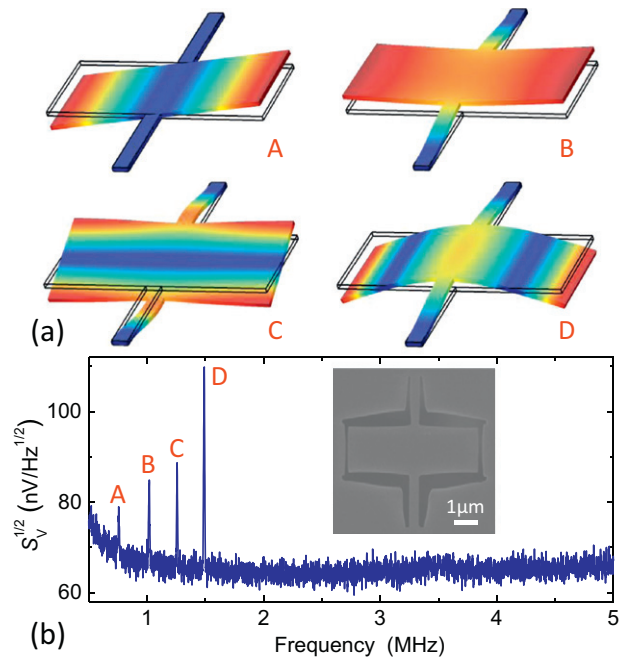


Fig. 6. (a) FEM simulation of the mode shapes of a nanocrystalline diamond multi-mode nanomechanical resonator device on 100 nm-thick film (dimension: paddle size $5\text{ }\mu\text{m} \times 2\text{ }\mu\text{m} \times 100\text{ nm}$; $l_T \approx 2\text{ }\mu\text{m}$; $w_T \approx 350\text{ nm}$). (b) Measured undriven, thermomechanical resonance of the torsional resonator with laser interferometry using 633 nm red laser at 0.35 mW laser power on device, and device is burned after the measurement. Voltage domain noise spectral density is shown in the 0.5–5 MHz range, where A–D correspond to the simulated resonance mode shapes in (a). Inset shows the SEM image of the device.

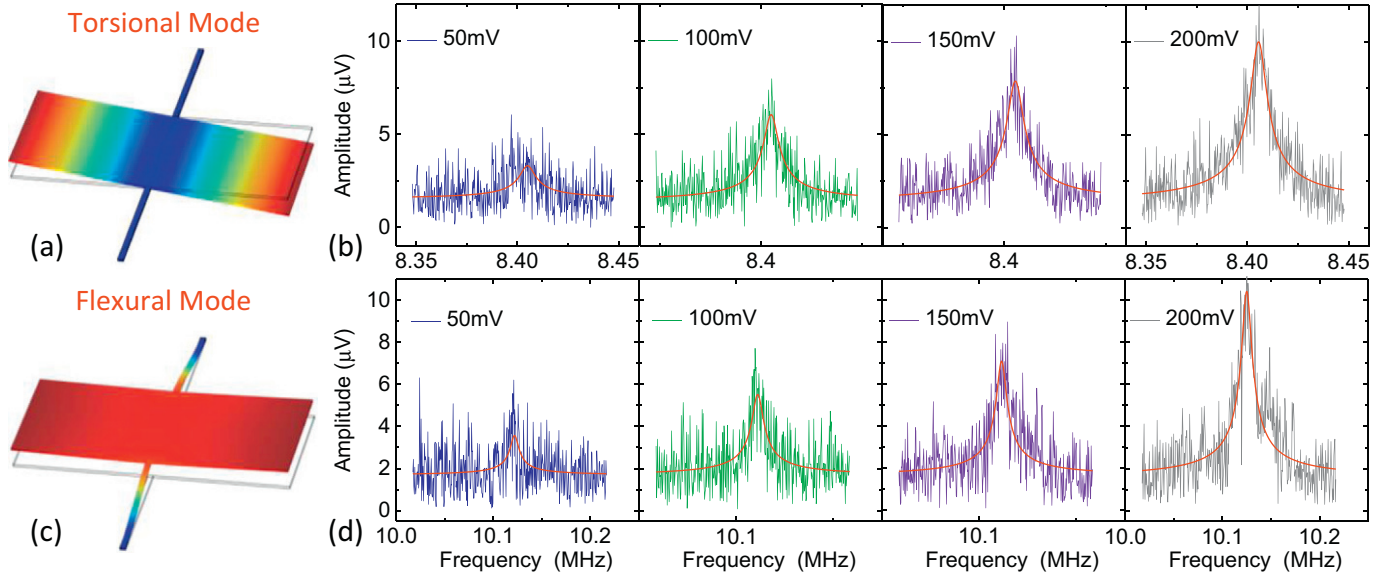


Fig. 7. FEM simulation of the mode shapes and sequences (a & c) and measured resonance spectra (b & d) of a 50 nm-thick nanocrystalline diamond torsional resonator with paddle size of $5\ \mu\text{m} \times 2\ \mu\text{m}$ and tether length $l_T \approx 2\ \mu\text{m}$, width $w_T \approx 90\ \text{nm}$ (device picture given in Fig. 3(d)), for (a & b) torsional mode, and (c & d) flexural mode resonance, under increasing optical driving amplitudes shown by different colors. Fittings show Q of 1100–1200 for the resonance in (b) and 900–1200 for the one in (d).

by a photodetector, which is then collected by the network analyzer and results in a resonance in the frequency spectrum.

4. Results and discussions

Figure 6 shows the multiple resonances associated with the undriven thermomechanical motion of a device fabricated from a 100 nm thick film. We perform FEM simulation to confirm the sequence of the resonance modes (Fig. 6(a)), matching the first 4 mode shapes with the measured resonances (Fig. 6(b)). A voltage domain power spectral density is recorded in the 0.5–5 MHz range; however, when we try to optimize the resonances, they disappear. For a wide bandgap material like diamond, we should be able to use large laser power because the absorption should be very small at the detection wavelength. However, when using an on-device laser power of 0.35 mW to record the spectrum in Fig. 6, we observe that the device is damaged due to excessive laser heating. This suggests the CVD diamond film contains a considerable amount of

amorphous carbon, graphite, or trans-polyacetylene, which could absorb a significant amount of laser power; a suggestion that is consistent with the Raman spectrum from the sample. When the laser power is reduced to 70 μW , the device is not damaged even after focusing the laser on the device for at least half an hour, thus enabling device characterization without inducing changes in the material.

With very small laser power, however, it would be difficult to detect the thermomechanical motion, and therefore we use optical driving to measure the resonance. Fig. 7 shows the measurements from a device made from a 50 nm film, with w_T as small as 90 nm. The resonance responses from both torsional and flexural modes are recorded, with different RF driving amplitudes indicated by different colors (Fig. 7(b) and (d)). The mode sequence is confirmed by the FEM simulation (Fig. 7(a) and (c)), where the first mode at $f_{\text{res}} = 8.4\ \text{MHz}$ is the torsional mode, and the second mode at $f_{\text{res}} = 10.12\ \text{MHz}$ is the flexural mode. The quality factors are obtained by fitting the resonance spectra to the model of a driven damped simple harmonic resonator [32], resulting in Q factors from 1100 to 1200 for the torsional mode, and 900–1200

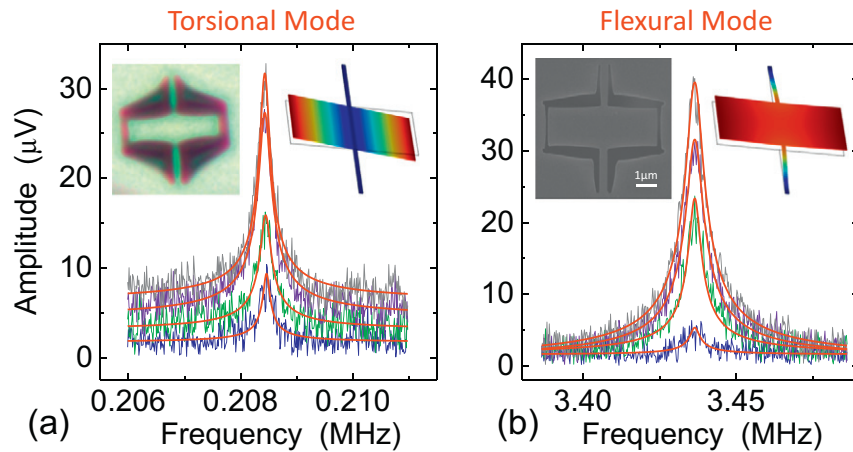


Fig. 8. Measured resonance spectra of a 100 nm-thick diamond torsional resonator with paddle size $5\ \mu\text{m} \times 2\ \mu\text{m}$; $l_T \approx 2\ \mu\text{m}$; $w_T \approx 400\ \text{nm}$ for its (a) torsional mode, and (b) flexural mode under different driving amplitudes. Colors indicate different optical driving amplitudes (blue: 20 mV, olive: 80 mV, violet: 140 mV, gray: 200 mV). Fittings give Q of 1000–1800 for the torsional resonance in (a) and 600–1100 for the flexural one in (b). Insets on the left: optical microscope image (a), and SEM image (b). Insets on the right: mode shapes and sequence from FEM simulation for torsional (a) and flexural (b) modes.

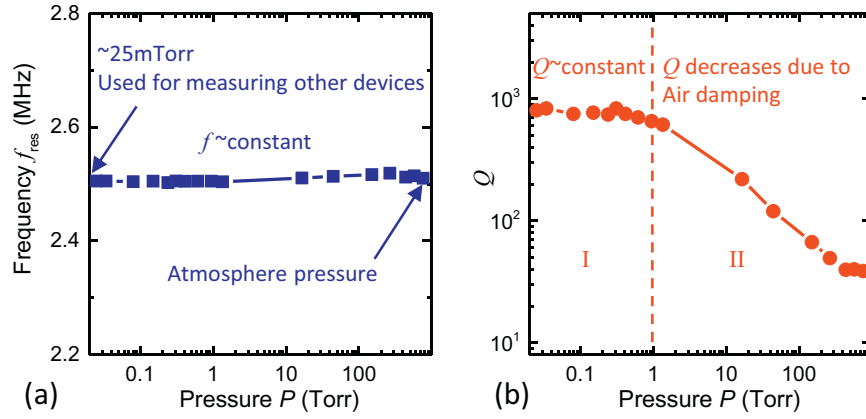


Fig. 9. Measured pressure dependence of (a) f_{res} and (b) Q of a torsional resonator on a 50 nm-thick nanocrystalline diamond film and with similar dimension as the device shown in Fig. 3d.

for the flexural mode, with different driving amplitudes resulting in different Q 's.

From the torsional resonance shown in Fig. 7(b), we extract E_Y using

$$E_Y = \frac{(2\pi f)^2 (\gamma_P + 1) L_T I}{J_T} \quad (6)$$

to obtain $E_Y = 977$ GPa. The torsional resonance is not affected by the built-in stress in the film, while the flexural mode resonance frequency depends on the stress along the axis defined by the tethers. The flexural mode resonance data is shown in Fig. 7(d); the signal amplitudes are similar to the torsional mode with laser position shown in Fig. 5. We also measure driven resonance for a device made from a 100 nm thick film, as shown in Fig. 8. Though the tether for this device is wider than a comparable device made from the 50 nm film ($w_T \approx 400$ nm), the resonance frequency is lower and the extracted E_Y is also quite small. The resonance frequency and the E_Y data are consistent with the Raman spectra, where the device exhibiting higher torsional mode resonance frequency and higher E_Y is of higher crystal quality as compared with the device with lower resonant frequency and lower E_Y . These data suggest that the variation in device performance could be due to the differences in microstructural quality resulting from the MPCVD growth process used to produce the films and/or run-to-run variation within the process.

In order to calibrate the pressure dependence of the torsional resonator, we record the resonance spectra of a 50 nm-thick device with dimensions similar to the device shown in Fig. 3d under conditions of varying pressure. We extract f_{res} and Q from vacuum (~ 25 mTorr) to atmospheric pressure (760 Torr), as shown in Fig. 9. We find that the resonance frequency of the device is quite stable, and the frequency variation is within ± 0.01 MHz. While Q decreases by ~ 20 times as the pressure is increased from 25 mTorr to atmosphere pressure, indicating that air damping is significant at higher pressure [42]. In particular, we observe that Q is relatively stable at pressures lower than 1 Torr (Region I in Fig. 9(b)), and then quickly decreases at pressures higher than 1 Torr (Region II in Fig. 9(b)), which suggests that our measurement range is sufficient for capturing the key performance characteristics of the device.

Table 1 compares the key performance parameters of some torsional resonators with the devices in this study. Among all the torsional resonators listed, our nanocrystalline diamond devices have the smallest thickness and tether width with the exception of the device reported in Ref [18] (Sample #4) which uses multiwalled carbon nanotubes as the tether material. While carbon nanotubes are chemically synthesized and usually require careful assembly, our nanocrystalline diamond devices are fabricated with FIB, and have higher resonance frequencies and Q 's. The resonance frequency is in the HF band, comparable with other torsional resonators at high frequencies (Sample #10). The Q 's of our devices are not yet optimized compared to other torsional resonators,

Table 1
Comparison of reported torsional resonators in material, dimensions, resonance frequency, and Q . The samples 14 and 15 show our previously published results, and the samples 16–18 show the device in this paper.

Sample #	Tether material	Torsional paddle dimension ($L \times w \times t$) μm^3	Tether dimension	Torsional resonance frequency f (MHz)	Q
1 [ref 20]	Si	Around $1 \times 2 \times 0.2$	$L_T \approx 1 \mu\text{m}$, $w_T = 200$ nm	2.61	6500
2 [ref 21]	Si	$4 \times 15 \times 0.2$	$w_T = 150\text{--}200$ nm	0.485	N/A
3 [ref 22]	Si	$2 \times 3 \times 0.2$	$L_T \approx 2 \mu\text{m}$, $w_T = 170$ nm	5.6	2500
4 [ref 23]	Multiwalled carbon nanotube	$0.5 \times 0.6 \times 0.14$	Diameter $d \approx 20$ nm	3.79	140
5 [ref 24]	Si	$98 \times 147 \times 1.5$	N/A	0.47	5.2×10^5
6 [ref 25]	Polysilicon	$106 \times 44 \times 1.5$	(Serpentine spring)	0.07	2.6×10^5
7 [ref 26]	SiN	$2 \times 5 \times 0.5$	$L_T \approx 2 \mu\text{m}$, $w_T = 200$ nm	6.626	5225
8 [ref 27]	Si	$5.8 \times 5.8 \times 0.3$	$L_T \approx 1.8 \mu\text{m}$, $w_T = 600$ nm	7.38	7775
9 [ref 28]	Silicon nitride	$2 \times 3.73 \times 0.1$	$w_T \approx 200$ nm	3.36 (first mode)	800 (first mode)
10 [ref 29]	Si	$1.5 \times 3.5 \times 0.215$	$L_T \approx 5 \mu\text{m}$, $w_T = 200$ nm	9.04	3800
11 [ref 30]	Si	$100 \times 250 \times 3$	$L_T \approx 300 \mu\text{m}$, $w_T = 100 \mu\text{m}$	0.525 (second mode)	1.1×10^4
12 [ref 31]	Si	$50 \times 50 \times 3$	$L_T \approx 300 \mu\text{m}$, $w_T = 30 \mu\text{m}$	0.05	91
13 [ref 11]	Polycrystalline diamond	$30 \times 5 \times 0.7$	$L_T \approx 20 \mu\text{m}$, $w_T = 500$ nm	0.53	3.5×10^4
14 [ref 32]	6H-SiC	Diameter $d \approx 5 \mu\text{m}$, $t \approx 1.2 \mu\text{m}$	$L_T \approx 2 \mu\text{m}$, $w_T = 700$ nm	57.1	280
15 [ref 33]	6H-SiC	Diameter $d \approx 15.9 \mu\text{m}$, $t \approx 1.2 \mu\text{m}$	$L_T \approx 2.05 \mu\text{m}$, $w_T = 2.1 \mu\text{m}$ (triangular cross section)	2.47	1250
16 [This work*]	Nanocrystalline diamond	$2 \times 5 \times 0.05$	$L_T \approx 2 \mu\text{m}$, $w_T = 90$ nm	8.4	1200
17 [This work*]	Nanocrystalline diamond	$2 \times 5 \times 0.1$	$L_T \approx 2 \mu\text{m}$, $w_T = 400$ nm	0.2084	1800
18 [This work*]	Nanocrystalline diamond	$2 \times 5 \times 0.1$	$L_T \approx 2 \mu\text{m}$, $w_T = 350$ nm	0.76	126

and thus should increase with further improvements in the process. Though torsional resonators based on polycrystalline diamond have been reported (Sample #13), the resonance frequency is not as high as that in our devices.

5. Conclusion

In conclusion, we have fabricated nanocrystalline diamond torsional resonators by using specifically engineered FIB and studied their interesting resonant characteristics in both torsional and flexural modes. By measuring intrinsic thermomechanical motions and driven resonances, we show multimode resonances with torsional resonance frequencies up to the HF band. We have also extracted Young's modulus from the resonance frequency of a 50 nm thick device and found that it is almost comparable to that of single crystal diamond. The findings reported herein could provide guidelines for designing high-performance resonant sensors suitable for harsh-environment applications based on the nanocrystalline diamond platform.

Prime novelty statement

For the first time, we demonstrate torsional nanomechanical resonators based on nanocrystalline diamond films as thin as 50 nm, exhibiting multiple resonance modes in the MHz range, and quality (Q) factors exceeding 1800 at room temperature in moderate vacuum (~20 mTorr).

Acknowledgments

We thank J. Lee, Z. Wang and L. Zhao for helpful discussions and technical assistance in the labs. We acknowledge the support from the Case School of Engineering and National Science Foundation (NSF) through Grant CMMI-1246715 (SNM), and the technical support from the Swagelok Center for Surface Analysis of Materials (SCSAM) at Case.

References

- [1] O. Auciello, J. Birrell, J.A. Carlisle, J.E. Gerbi, X. Xiao, B. Peng, H.D. Espinosa, Materials science and fabrication processes for a new MEMS technology based on ultrananocrystalline diamond thin films, *J. Phys. Condens. Matter* 16 (2004) R539–R552.
- [2] L. Sekaric, J.M. Parpia, H.G. Craighead, T. Feygelson, B.H. Houston, J.E. Butler, Nanomechanical resonant structures in nanocrystalline diamond, *Appl. Phys. Lett.* 81 (2002) 4455–4457.
- [3] J. Philip, P. Hess, T. Feygelson, J.E. Butler, S. Chattopadhyay, K.H. Chen, L.C. Chen, Elastic, mechanical, and thermal properties of nanocrystalline diamond films, *J. Appl. Phys.* 93 (2003) 2164–2171.
- [4] E. Kohn, P. Gluche, M. Adamschik, Diamond MEMS—a new emerging technology, *Diamond Relat. Mater.* 8 (1999) 934–940.
- [5] N. Sepulveda, D. Aslam, J.P. Sullivan, Polycrystalline diamond MEMS resonator technology for sensor applications, *Diamond Relat. Mater.* 15 (2006) 398–403.
- [6] N. Sepulveda, J. Lu, D.M. Aslam, J.P. Sullivan, High-performance polycrystalline diamond micro- and nanoresonators, *J. Microelectromech. Syst.* 17 (2008) 473–482.
- [7] M. Akgul, R. Schneider, Z. Ren, G. Chandler, V. Yeh, C.T.-C. Nguyen, Hot filament CVD conductive microcrystalline diamond for high Q, high acoustic velocity micromechanical resonators, 2011 IEEE Int. Joint Conf. of Freq. Control and the European Freq. and Time Forum (IFCS' 11), 2011, pp. 1–6.
- [8] V.P. Adiga, A.V. Sumant, S. Suresh, C. Gudeman, O. Auciello, J.A. Carlisle, R.W. Carpick, Mechanical stiffness and dissipation in ultrananocrystalline diamond microresonators, *Phys. Rev. B* 79 (2009) 245403.
- [9] J. Wang, J.E. Butler, D.S.Y. Hsu, C.T.-C. Nguyen, CVD polycrystalline diamond high-Q micromechanical resonators, 15th IEEE Int. Conf. on Micro Electro Mechanical Systems (MEMS' 02), 2002, pp. 657–660.
- [10] J. Wang, J.E. Butler, T. Feygelson, C.T.-C. Nguyen, 1.51-GHz nanocrystalline diamond micromechanical disk resonator with material-mismatched isolating support, 17th IEEE Int. Conf. on Micro Electro Mechanical Systems (MEMS' 04), 2004, pp. 641–644.
- [11] N. Sepulveda, D.M. Aslam, J.P. Sullivan, J.R. Wendt, B.B. McKenzie, Polycrystalline diamond micromechanical resonators with nanometer dimensions, 1st IEEE Int. Conf. on Nano/Micro Engineered and Molecular Systems (NEMS '06), 2006, pp. 662–667.
- [12] H. Najar, M.-L. Chan, H.-A. Yang, L. Lin, D.G. Cahill, D.A. Horsley, High quality factor nanocrystalline diamond micromechanical resonators limited by thermoelastic damping, *Appl. Phys. Lett.* 104 (2014) 151903.
- [13] H. Najar, A. Heidari, M.-L. Chan, H.-A. Yang, L. Lin, D.G. Cahill, D.A. Horsley, Microcrystalline diamond micromechanical resonators with quality factor limited by thermoelastic damping, *Appl. Phys. Lett.* 102 (2013) 071901.
- [14] M. Imboden, O.A. Williams, P. Mohanty, Observation of nonlinear dissipation in piezoresistive diamond nanomechanical resonators by heterodyne down-mixing, *Nano Lett.* 13 (2013) 4014–4019.
- [15] A. Gaidarzhy, M. Imboden, P. Mohanty, J. Rankin, B.W. Sheldon, High quality factor gigahertz frequencies in nanomechanical diamond resonators, *Appl. Phys. Lett.* 91 (2007) 203503.
- [16] M. Imboden, O.A. Williams, P. Mohanty, Nonlinear dissipation in diamond nanoelectromechanical resonators, *Appl. Phys. Lett.* 102 (2013) 103502.
- [17] M. Imboden, P. Mohanty, A. Gaidarzhy, J. Rankin, B.W. Sheldon, Scaling of dissipation in megahertz-range micromechanical diamond oscillators, *Appl. Phys. Lett.* 90 (2007) 173502.
- [18] R.A. Johnson, *Mechanical Filters in Electronics*, John Wiley & Sons Inc., New York, 1983.
- [19] A.N. Cleland, *Foundations of Nanomechanics*, Springer, Berlin, 2003.
- [20] A.N. Cleland, M.L. Roukes, A nanometre-scale mechanical electrometer, *Nature* 392 (1998) 160–162.
- [21] D.W. Carr, S. Evoy, L. Sekaric, H.G. Craighead, J.M. Parpia, Parametric amplification in a torsional microresonator, *Appl. Phys. Lett.* 77 (2000) 1545–1547.
- [22] A. Olkhovets, S. Evoy, D.W. Carr, J.M. Parpia, H.G. Craighead, Actuation and internal friction of torsional nanomechanical silicon resonators, *J. Vac. Sci. Technol. B* 18 (2000) 3549–3551.
- [23] S.J. Papadakis, A.R. Hall, P.A. Williams, L. Vicci, M.R. Falvo, R. Superfine, S. Washburn, Resonant oscillators with carbon-nanotube torsion springs, *Phys. Rev. Lett.* 93 (2004) 146101.
- [24] B.H. Houston, D.M. Photiadis, J.F. Vignola, M.H. Marcus, X. Liu, D. Czaplowski, L. Sekaric, J. Butler, P. Pehrsson, J.A. Bucaro, Loss due to transverse thermoelastic currents in microscale resonators, *Mater. Sci. Eng.* 370 (2004) 407–411.
- [25] D. Antonio, H. Pastoriza, Nonlinear dynamics of a micromechanical torsional resonator: analytical model and experiments, *J. Microelectromech. Syst.* 18 (2009) 1396–1400.
- [26] X.C. Zhang, E.B. Myers, J.E. Sader, M.L. Roukes, Nanomechanical torsional resonators for frequency-shift infrared thermal sensing, *Nano Lett.* 13 (2013) 1528–1534.
- [27] J. Losby, J.A.J. Burgess, Z. Diao, D.C. Fortin, W.K. Hiebert, M.R. Freeman, Thermomechanical sensitivity calibration of nanotorsional magnetometers, *J. Appl. Phys.* 111 (2012) 07D305.
- [28] J.P. Davis, D. Vick, D.C. Fortin, J.A.J. Burgess, W.K. Hiebert, M.R. Freeman, Nanotorsional resonator torque magnetometry, *Appl. Phys. Lett.* 96 (2010) 072513.
- [29] P.H. Kim, C. Doolin, B.D. Hauer, A.J.R. MacDonald, M.R. Freeman, P.E. Barclay, J.P. Davis, Nanoscale torsional optomechanics, *Appl. Phys. Lett.* 102 (2013) 053102.
- [30] X. Xia, Z. Zhang, X. Li, A Latin-cross-shaped integrated resonant cantilever with second torsion-mode resonance for ultra-resoluble bio-mass sensing, *J. Micromech. Microeng.* 18 (2008) 035028.
- [31] O. Sahin, S. Magonov, C. Su, C.F. Quate, O. Solgaard, An atomic force microscope tip designed to measure time-varying nanomechanical forces, *Nat. Nanotechnol.* 2 (2007) 507–514.
- [32] R. Yang, Z. Wang, J. Lee, K. Ladhane, D.J. Young, P.X.-L. Feng, 6H-SiC microdisk torsional resonators in a “smart-cut” technology, *Appl. Phys. Lett.* 104 (2014) 091906.
- [33] R. Yang, K. Ladhane, Z. Wang, J. Lee, D.J. Young, P.X.-L. Feng, Smart-cut 6H-silicon carbide (SiC) microdisk torsional resonators with sensitive photon radiation detection, 27th IEEE Int. Conf. on Micro Electro Mechanical Systems (MEMS' 14), 2014, pp. 793–796.
- [34] S. Timoshenko, *Vibration Problems in Engineering*, D. Van Nostrand Company, Inc., New York, 1937.
- [35] W.C. Young, R.G. Budynas, *Roark's Formulas for Stress and Strain*, McGraw-Hill, New York, 2002.
- [36] J.M. Gere, B.J. Goodno, *Mechanics of Materials*, Cengage Learning, Stamford, 2013.
- [37] A.C. Barnes, C.A. Zorman, Polycrystalline diamond circular resonant diaphragms with low onset of nonlinear response, 2013 IEEE Sensors, 2013, pp. 1–4.
- [38] D.S. Knight, W.B. White, Characterization of diamond films by Raman spectroscopy, *J. Mater. Res.* 4 (1989) 385–393.
- [39] S.A. Solin, A.K. Ramdas, Raman spectrum of diamond, *Phys. Rev. B* 1 (1970) 1687–1698.
- [40] H. Kuzmany, R. Pfeiffer, N. Salk, B. Gunther, The mystery of the 1140 cm⁻¹ Raman line in nanocrystalline diamond films, *Carbon* 42 (2004) 911–917.
- [41] R. Yang, Z. Wang, J. Lee, K. Ladhane, D.J. Young, P.X.-L. Feng, Temperature dependence of torsional and flexural modes in 6H-SiC microdisk resonators, 2014 IEEE Int. Freq. Control Symposium (IFCS' 14), 2014, pp. 1–3.
- [42] J. Lee, Z. Wang, K. He, J. Shan, P.X.-L. Feng, Air damping of atomically thin MoS₂ nanomechanical resonators, *Appl. Phys. Lett.* 105 (2014) 023104.